

Probing quantum complexity via universal saturation of stabilizer entropies

Tobias Haug^{1,2}, Leandro Aolita¹, and M.S. Kim²

¹Quantum Research Center, Technology Innovation Institute, Abu Dhabi, UAE

²Blackett Laboratory, Imperial College London SW7 2AZ, UK

July 15, 2024

Nonstabilizerness or ‘magic’ is a key resource for quantum computing and a necessary condition for quantum advantage. Non-Clifford operations turn stabilizer states into resourceful states, where the amount of nonstabilizerness is quantified by resource measures such as stabilizer Rényi entropies (SREs). Here, we show that SREs saturate their maximum value at a critical number of non-Clifford operations. Close to the critical point SREs show universal behavior. Remarkably, the derivative of the SRE crosses at the same point independent of the number of qubits and can be rescaled onto a single curve. We find that the critical point depends non-trivially on Rényi index α . For random Clifford circuits doped with T-gates, the critical T-gate density scales independently of α . In contrast, for random Hamiltonian evolution, the critical time scales linearly with qubit number for $\alpha > 1$, while is a constant for $\alpha < 1$. This highlights that α -SREs reveal fundamentally different aspects of nonstabilizerness depending on α : α -SREs with $\alpha < 1$ relate to Clifford simulation complexity, while $\alpha > 1$ probe the distance to the closest stabilizer state and approximate state certification cost via Pauli measurements. As technical contributions, we observe that the Pauli spectrum of random evolution can be approximated by two highly concentrated peaks which allows us to compute its SRE. Further, we introduce a class of random evolution that can be expressed as random Clifford circuits and rotations, where we provide its exact SRE. Our results opens up new approaches to characterize the complexity of quantum systems.

1 Introduction

Nonstabilizerness or ‘magic’ has been proposed as the resource theory of fault-tolerant quantum computers [48]. It lower bounds the non-Clifford resources needed to run quantum computers [24] and relates

to the complexity of classical simulation algorithms based on Clifford operations [3].

Nonstabilizerness monotones are non-increasing under Clifford operations, while applying non-Clifford operations can enhance the amount of nonstabilizerness of a state. On a quantitative level, the relationship between quantum complexity and number of non-Clifford operations is an intensely studied topic [16, 28, 33]. As nonstabilizerness is a measure of complexity for quantum computers and a necessary condition for quantum advantage, it is paramount to understand how nonstabilizerness depends on the number of non-Clifford operations [7, 33, 43, 49].

A wide range of magic monotones have been proposed, such as stabilizer rank [3], min-relative entropy of magic [4, 33] and log-free robustness of magic [24, 33]. These measures probe different aspects of nonstabilizerness. In particular, the log-free robustness of magic can be related to the complexity of a classical simulation algorithm, while the min-relative entropy of magic is related to the distance to the closest stabilizer state. However, they require an optimization program to be computed, making them in general intractable for the study of larger system sizes. Thus, methods to feasibly approximate these monotones are desired.

α -Stabilizer Rényi entropies (SREs) have been proposed to quantitatively explore nonstabilizerness harnessing their efficient numerical [19, 25, 29], analytic [34, 46] and experimental accessibility [1, 18, 22, 38]. Here, the Rényi index α indicates the moment of the SRE. They are monotones for pure states for $\alpha \geq 2$ [27], while monotonicity can be violated for $\alpha < 2$ [20]. SREs relate to phases of error-corrected circuits [36], quantify the entanglement spectrum [45], bound fidelity estimation [23, 30, 31], characterize the robustness of shadow tomography [5] and characterize pseudorandom states [12, 21]. Further, SREs characterize many-body phenomena [13] such as phase transitions [19, 44], frustration [37], random matrix product states [9, 26, 35, 40], localization [47] and out-of-time-order correlators [10, 28, 30]. SREs also lower bound other intractable magic monotones [20, 22].

Here, we study α -SREs for random Clifford circuits doped with T-gates, as well as random Hamiltonian

Tobias Haug: tobias.haug@u.nus.edu

evolution in time. We reveal that SREs saturate their maximal value at a critical T-gate density $q_{c,\alpha}$ or critical time $t_{c,\alpha}$ in the thermodynamic limit. Around the critical point, the the SRE become universal, which we demonstrate by the derivative of the SRE crossing at the critical point for all number of qubits N . Further, by a simple rescaling we can collapse the derivative to a single curve, hinting at a possible connection to phase transitions.

For random Clifford circuits doped with T-gates, SREs grow linearly with number of T-gates until reaching a critical T-gate density which is independent of number of qubits N for any α . In contrast, for random Hamiltonian evolution $\alpha < 1$ SREs increase exponentially at short times, becoming extensive already at $1/\text{poly}(N)$ time. In contrast, $\alpha > 1$ SREs grow independent of N with a critical time that is linear with N , which we find to be a tight lower bound of the stabilizer fidelity.

We argue that $\alpha > 1$ and $\alpha < 1$ probe different aspects of nonstabilizerness and relate to different quantum computational tasks. $\alpha < 1$ SREs (especially $\alpha = 1/2$) relate to the number of superpositions of stabilizer states needed to represent a given state which characterizes the cost of Clifford-based simulation algorithms as well as cost of fault-tolerant state preparation. In contrast, $\alpha > 1$ SREs can be seen as the distance to the closest stabilizer state which for example characterizes the cost of Pauli-based fidelity certification.

We argue that Clifford simulation and state certification become inefficient at the same T-gate doping for Clifford circuits. In contrast, for random evolution these two tasks have completely distinct timescales. In particular, Clifford simulation of random Hamiltonian evolution becomes difficult beyond exponentially small times, while (approximate) state certification is possible up to constant times.

Thus, while both Clifford simulation and state certification with Pauli measurements are intrinsically linked to nonstabilizerness, the efficiency of these tasks is in general not correlated. Their efficiency depends on two very different aspects of nonstabilizerness, which can be probed with α -SREs.

As technical contributions, we show that random Hamiltonian evolution has a Pauli spectrum with two distinct peaks, which allows us to compute its SRE. We also introduce a type of random evolution which can be expressed as Clifford circuits with small rotations, which possesses an analytic form of the SRE for $\alpha = 2$.

Our main results are summarized in Fig. 1 and the critical T-gate density and time are summarized in Table 1.

Index	Random Clifford+T
$\alpha \leq 2$	$q_{c,\alpha} \approx (1 - \alpha) \frac{\ln(2)}{\ln(2^{-\alpha + \frac{1}{2}})}$
$\alpha > 2$	$q_{c,\alpha} \approx -\frac{\ln(2)}{\ln(2^{-\alpha + \frac{1}{2}})}$
Random evolution	
$\alpha = 0$	$t_{c,\alpha}^2 = 0$
$0 < \alpha < 1$	$t_{c,\alpha}^2 \approx \frac{1}{2}$
$1 < \alpha \leq 2$	$t_{c,\alpha}^2 \approx -\frac{1-\alpha}{2\alpha} N \ln(2)$
$\alpha > 2$	$t_{c,\alpha}^2 \approx \frac{1}{2\alpha} N \ln(2)$

Table 1: Critical T-gate density $q_{c,\alpha}$ for random Clifford circuits doped with T-gates and critical time $t_{c,\alpha}$ for evolution with random Hamiltonians. At $q_{c,\alpha}$ and $t_{c,\alpha}$, SREs converge to their maximal value for $N \gg 1$.

2 Stabilizer Rényi entropy

For an N -qubit state $|\psi\rangle$, the α -SRE is given by [29]

$$M_\alpha(|\psi\rangle) = (1 - \alpha)^{-1} \ln(2^{-N} \sum_{\sigma \in \mathcal{P}} \langle \psi | \sigma | \psi \rangle^{2\alpha}). \quad (1)$$

where α is the index of the SRE and $\mathcal{P} = \{\sigma\}_\sigma$ is the set of all 4^N Pauli strings $\sigma \in \{I, X, Y, Z\}^N$ which are tensor products of Pauli matrices. We note the limit $\alpha \rightarrow 1$, which can be easily shown using l'Hôpital's rule and is called the von Neumann stabilizer entropy [20]

$$M_1(|\psi\rangle) = -2^{-N} \sum_{\sigma \in \mathcal{P}} \langle \psi | \sigma | \psi \rangle^2 \ln(\langle \psi | \sigma | \psi \rangle^2). \quad (2)$$

For convenience, we also define the SRE density

$$m_\alpha = M_\alpha / N. \quad (3)$$

M_α is a resource measure of nonstabilizerness for pure states [48]. SREs are faithful, i.e. $M_\alpha = 0$ only for pure stabilizer states, while $M_\alpha > 0$ for all other states. Further, M_α is a monotone for $\alpha \geq 2$ [27], i.e. non-increasing under free operations, which are Clifford operations that map pure states to pure states. Note that for $\alpha < 2$ SREs can violate the monotonicity condition [20]. For all α , SREs are invariant under Clifford unitaries U_C , i.e. $M_\alpha(U_C |\psi\rangle) = M_\alpha(|\psi\rangle)$. SREs are also additive with $M_\alpha(|\psi\rangle \otimes |\phi\rangle) = M_\alpha(|\psi\rangle) + M_\alpha(|\phi\rangle)$. Note that M_α are not strong monotones for any α [20]. As Rényi entropies, SREs are monotonously increasing with decreasing α , i.e.

$$N \ln(2) \geq M_\alpha \geq M_{\alpha'} \geq 0 \quad (4)$$

for $\alpha < \alpha'$.

As other nonstabilizerness monotones, we also consider the min-relative entropy of magic [4, 33]

$$D_{\min}(|\psi\rangle) = -\log \left(\max_{|\phi\rangle \in \text{STAB}} |\langle \psi | \phi \rangle|^2 \right), \quad (5)$$

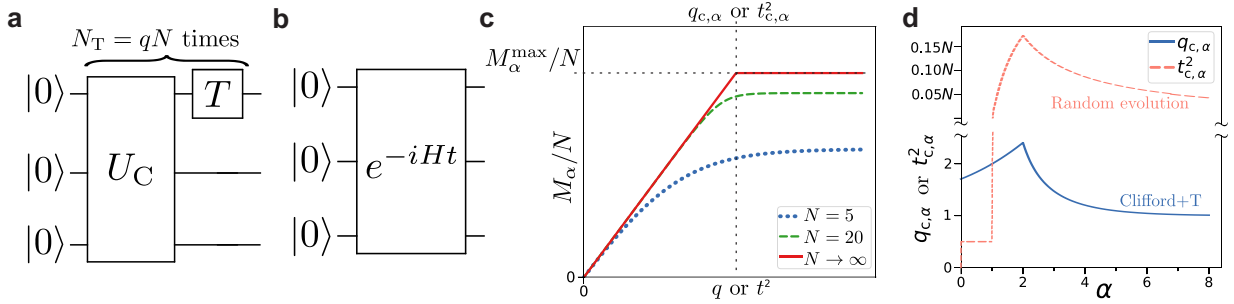


Figure 1: Overview of main results. We study two models: **a**) Circuits composed of randomly chosen Clifford circuits U_C doped with $N_T = qN$ T-gates, where N is the number of qubits and q the T-gate density. **b**) Evolution in time t for random Hamiltonians starting from an initial stabilizer state. **c**) α -stabilizer Rényi entropy (SRE) M_α increases monotonously with q and t until converging to a constant. For large N we observe a sharp transition to maximal SRE M_α^{\max} (horizontal dashed line) for a critical T-gate density $q_{c,\alpha}$ or critical time $t_{c,\alpha}$ (vertical dashed line). The derivative of M_α crosses at the critical point for all N and the dynamics close to the critical point can be mapped onto a single curve (see Fig.2 and Fig. 4). **d**) Critical T-gate density $q_{c,\alpha}$ and time $t_{c,\alpha}$ as function of Rényi index α . Both $q_{c,\alpha}$ and $t_{c,\alpha}$ vary non-monotonously with α as they probe different aspects of nonstabilizerness complexity. In particular, critical time $t_{c,\alpha}$ changes its scaling from constant ($\alpha < 1$) to $t_{c,\alpha} \sim \sqrt{N}$ ($\alpha > 1$).

where the maximum is taken over the set of pure stabilizer states. Here, $F_{\text{STAB}} = \max_{|\phi\rangle \in \text{STAB}} |\langle \psi | \phi \rangle|^2$ is the stabilizer fidelity. D_{\min} measures the distance between $|\psi\rangle$ and its closest stabilizer state. It is upper bounded by $D_{\min} \leq N \ln(2)$, which is asymptotically reached for Haar random states [33]. The SRE lower bounds D_{\min} for $N > 1$

$$D_{\min}(|\psi\rangle) \geq \frac{\alpha - 1}{2\alpha} M_\alpha(|\psi\rangle) \quad (\alpha > 1). \quad (6)$$

We also consider the log-free robustness of magic [24, 33]

$$\text{LR}(\rho) = \log \left[\min_x \left\{ \sum_i |x_i| : \rho = \sum_i x_i \eta_i \right\} \right], \quad (7)$$

where $S = \{\eta_i\}_i$ is the set of pure N -qubit stabilizer states. The SRE lower bounds the log-free robustness for $\alpha \geq 1/2$ [24, 29]

$$\text{LR}(|\psi\rangle) \geq \frac{1}{2} M_\alpha(|\psi\rangle) \quad (\alpha \geq 1/2). \quad (8)$$

Finally, the SRE is a lower bound to the stabilizer nullity $\nu \geq M_\alpha$ which is given by

$$\nu(|\psi\rangle) = N \ln(2) - \ln(s(|\psi\rangle)) \quad (9)$$

where $s(|\psi\rangle) = |\{\sigma : \langle \psi | \sigma | \psi \rangle^2 = 1\}|$ being the size of the set of all Pauli operators that stabilize $|\psi\rangle$.

3 Clifford circuits with T-gates

We now study the SRE for random circuits composed of Clifford unitaries and T-gates [16]. We consider a circuit of N_T layers consisting of randomly sampled Clifford circuits $U_C^{(k)}$ and the single-qubit T-gate $T = \text{diag}(1, \exp(-i\pi/4))$

$$|\psi(N_T)\rangle = U_C^{(0)} \left[\prod_{k=1}^{N_T} (T \otimes I_{N-1}) U_C^{(k)} \right] |0\rangle. \quad (10)$$

For $N_T = 0$, we have Clifford states, while for $N_T \sim N$ we have highly random states [28].

Analytic SRE. The average SRE of such states is known exactly for $\alpha = 2$ [29]

$$M_2(N_T) = -\ln \left[\frac{4 + (2^N - 1) \left(\frac{-4 + 3(4^N - 2^N)}{4(4^N - 1)} \right)^{N_T}}{(3 + 2^N)} \right] \quad (11)$$

For $N \gg 1$, this simplifies to

$$M_2(q) \approx -\ln \left[4 \times 2^{-N} + \left(\frac{3}{4} \right)^{qN} \right], \quad (12)$$

where we defined the T-gate density $q = N_T/N$. We study the SRE density $m_2 = M_2/N$ in Fig.2a for different N . We observe that m_2 increases linearly with q and converges to a constant for large q . For large N , we observe that the convergence appears to be a sharp transition to the maximal SRE $m_2 = \ln(2)$ which occurs at a critical T-gate density $q_{c,2}$. We determine $q_{c,2}$ by studying the scaling at finite N [39]. We find that $\partial_q m_2$ as function of q exhibits scale-invariant properties, i.e. the curves for different N can be mapped onto each other by appropriate rescaling around the critical point, a hallmark for phase transitions [39]. In particular, we find that $\partial_q m_2$ intersects for all N at the same point, which gives us $q_{c,2}$. Using Eq. (12), we find that the intersection occurs for all N at the critical T-gate density

$$q_{c,2} = \ln(2) / \ln\left(\frac{4}{3}\right) \approx 2.40942. \quad (13)$$

In Fig.2b we plot the derivative $\partial_q m_2$, observing that for all N the curves indeed intersect at $q_{c,2}$. In Fig.2c, we observe that by shifting q with $q_{c,2}$ and rescaling with N , we can collapse the curves of different N , as expected for the scale-invariant behavior close to critical points [39].

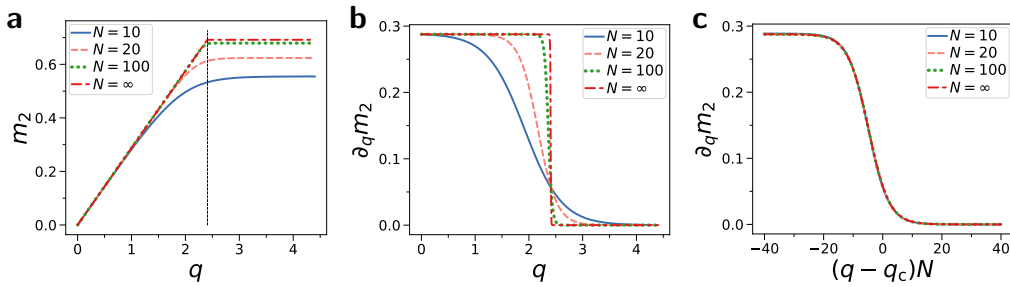


Figure 2: Universal behavior of 2-SRE for random Clifford + T circuits. **a)** m_2 against T-gate density $q = N_T/N$ for different N . Black vertical dashed line is transition T-gate density $q_{c,2} = \ln(2)/\ln(4/3)$ **b)** Derivative of SRE in respect to T-gate density $\partial_q m_2$ against q with universal crossing for all N at critical $q_{c,2} = \ln(2)/\ln(\frac{4}{3})$. **c)** Collapse of $\partial_q m_2$ against q when shifted by $q_{c,2}$ and scaled by N . Close to the critical density $q_{c,2}$, curves for different N intersect at a single point and can be mapped onto each other by a simple rescaling, which is hallmark of universality.

Next, we investigate the case $\alpha = 0$

$$M_0(|\psi\rangle) = \ln\left(\sum_{\sigma} \Theta(\langle\psi|\sigma|\psi\rangle^2)\right) - N \ln(2) \quad (14)$$

where $\Theta(x)$ is the Heaviside function with $\Theta(x) = 0$ for $x \leq 0$ and $\Theta(x) = 1$ for $x > 0$. Stabilizer states are stabilized by a commuting subgroup G of 2^N Pauli strings with $|\psi\rangle\sigma|\psi\rangle^2 = 1$ for $\sigma \in G$. The group G has N generators. Applying a T-gate on a stabilizer state breaks at most one generator of G , resulting in a state with $N-1$ generators and 2^{N-1} stabilizing Pauli strings. In fact, each additional T-gate can break only one generator. Thus, we find $M_0 \leq N_T \ln(2)$ and $M_0 \leq N \ln(2)$ [29]. When the T-gate is applied after a random Clifford circuit, the T-gate will break one of the generators of G with overwhelming probability. Thus, with overwhelming probability $N_T \approx N$ T-gates are necessary and sufficient to reach $M_0 = 0$, thus the critical T-gate density is $q_{c,0} = 1$.

Approximation of SRE. We now provide an estimate for the transition for other α . A single T-gate applied on a Clifford state gives an SRE of $M_\alpha^T = (1-\alpha)^{-1} \ln(2^{-\alpha} + \frac{1}{2})$. For $\alpha = 0$, each additional T-gate increases M_0 by the same amount M_0^T , yielding $M_0 = N_T M_0^T$ until reaching the maximum $M_0^{\max} = N_T M_0^T$ for $N_T = N$.

We find a similar analytic relationship for $\alpha = 2$. In particular, for large $N \gg 1$, Eq. (11) shows that each additional T-gate increases M_2 by M_2^T until the SRE is maximal. Thus, we have $M_2 \approx N_T M_2^T$, where N_T is the number of applied T-gates. As shown in Fig. 3a, we observe numerically that this linear relationship between M_α and N_T also applies for other α , i.e.

$$M_\alpha(N_T) \approx N_T M_\alpha^T. \quad (15)$$

The critical T-gate density $q_{c,\alpha}$ is reached when the SRE becomes maximal, which we can approximate with

$$q_{c,\alpha} \approx \frac{1}{N} M_\alpha^{\max} / M_\alpha^T. \quad (16)$$

Next, we estimate the value of the maximal SRE for $N \gg 1$. First, we recall the fact that nonstabilizerness

approaches the asymptotically the maximal possible value for randomly chosen states [33]. Thus, by estimating the SRE of a random state for large N we can approximate M_α^{\max} . A random state is spread out over the whole Pauli spectrum where for simplicity we assume a uniform distribution with $\langle\psi|\sigma|\psi\rangle^2 = 2^{-N}$ for $\sigma \in \mathcal{P}/\{I\}$. While such a state is not a positive density matrix, we find from numerical studies that this spectrum is a sufficiently good approximation of an actual random Pauli spectrum for large N . Using this ansatz, we find

$$\begin{aligned} M_\alpha^{\max} &\approx M_\alpha^{\text{uniform}} = (1-\alpha)^{-1} \ln(2^{-N} \sum_{\sigma \in \mathcal{P}} \langle\psi|\sigma|\psi\rangle^{2\alpha}) \\ &= (1-\alpha)^{-1} \ln(2^{-N} (1 + (4^N - 1)2^{-N\alpha})) \\ &\approx (1-\alpha)^{-1} \ln(2^{-N} + 2^{N(1-\alpha)}) \end{aligned}$$

This result is confirmed by the average $M_\alpha(|\psi_{\text{Haar}}\rangle)$ for Haar random states which has been computed in Ref. [46], where Haar random states are known to have asymptotically maximal nonstabilizerness [33]. Now, in the limit $N \gg 1$ we find

$$\begin{aligned} \alpha \leq 2: & \quad M_\alpha^{\max} \approx N \ln(2) \\ \alpha > 2: & \quad M_\alpha^{\max} \approx - (1-\alpha)^{-1} N \ln(2) \end{aligned} \quad (17)$$

Note that our result matches numerical simulations shown in Fig. 3b and the analytical values known for $\alpha = 0$ and $\alpha = 2$. We can now compute the critical T-gate density by inserting Eq. (17) into Eq. (16)

$$\begin{aligned} \alpha \leq 2: & \quad q_{c,\alpha} \approx (1-\alpha) \frac{\ln(2)}{\ln(2^{-\alpha} + \frac{1}{2})} \\ \alpha > 2: & \quad q_{c,\alpha} \approx - \frac{\ln(2)}{\ln(2^{-\alpha} + \frac{1}{2})}. \end{aligned} \quad (18)$$

4 Random basis evolution

We proceed to investigate another circuit model which can be seen as a type of random time evolution. It consist of a deep Clifford circuit as in Eq. (10) with

many layers d , but replace the T-gates with a parameterized rotation $R_z(\theta) = \exp(-i\theta/2\sigma_z)$. A similar model with randomly chosen θ has been shown to produce highly random states [15]. Here, instead we choose very small θ . In particular, we choose $\theta = 2t/\sqrt{d}$ with $d \gg N$

$$|\psi_c(t)\rangle = U_C^{(0)} \prod_{k=1}^d (R_z(\frac{2}{\sqrt{d}}) \otimes I_{N-1}) U_C^{(k)} |0\rangle. \quad (19)$$

Here, we can interpret t as evolution time. We argue that this circuit model describes a type of (time-dependent) random evolution: In particular, if we regard one layer, it consists of transformation into a random basis with Clifford $U_C^{(k)}$ and z -rotation in the transformed basis by small angle $\theta = 2t/\sqrt{d}$. This can be seen as a kind of a trotterized evolution with time-dependent Hamiltonian $H(t)$ which rapidly changes between different bases. We find numerically that the dynamics matches closely the evolution time of random Hamiltonians as shown in Appendix A.

For $t = 0$, Eq. 19 gives a Clifford state $|0\rangle$, while for $t \sim \sqrt{N}$ the SRE converges to the average value of the SRE for Haar random states. We compute M_2 for Eq. (19) analytically using the result of Ref. [29]

$$M_2(\theta, d, N) = -\ln[(3 + 2^N)^{-1}(4 + (2^N - 1) \times \left[\frac{7 \cdot 2^{2N} - 3 \cdot 2^N + 2^N(2^N + 3) \cos(4\theta) - 8}{8(2^{2N} - 1)} \right]^d)]. \quad (20)$$

In the limit of $N \gg 1$, $d \gg N$ and using $\theta = \frac{2t}{\sqrt{d}}$, we find approximately

$$M_2(t) \approx N \ln(2) - \ln(4 + 2^N e^{-4t^2}) \quad (21)$$

giving us

$$M_2(t) \approx 4t^2 \quad (22)$$

for $t \ll \sqrt{N}$. We confirm this scaling in Fig.4a.

Similar to circuits with Clifford and T-gates, we find a transition in the SRE when it converges to its maximum. In particular, we observe that the

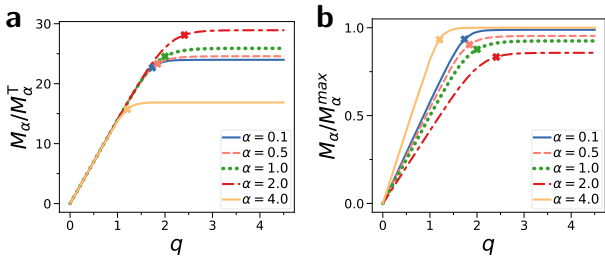


Figure 3: Saturation of α -SREs for random Clifford circuits doped with T-gates. **a)** M_α divided by α -SRE per T-gate M_α^T against T-gate density q . The crosses denote the critical T-gate density $q_{c,\alpha}$ as derived in Eq. (18). **b)** M_α divided by maximal SRE M_α^{\max} from Eq. (17) derived for $N \gg 1$. We show $N = 14$ qubits.

derivative $\partial_{t^2} M_2(t)$ in respect to t^2 intersects at $t_c^2 = \frac{1}{4} N \ln(2)$ for all N as shown in Fig.4b. We observe that the curves collapse onto a single line when shifted by t_c^2 in Fig.4c, demonstrating its scale-invariant behavior.

Finally, we study the circuit model for the min-relative entropy of magic Eq. (5). From numerically studies of our deep circuit model up to $N \leq 5$, we find that

$$D_{\min}(t) \approx t^2 \quad (23)$$

up to a time $t_c^2 \approx N \ln(2)$, where it then converges to the average value of Haar random states (see Appendix B). From the bound Eq. (6) we have for $\alpha = 2$ [20]

$$D_{\min}(t) \geq \frac{1}{4} M_2(t) \approx t^2, \quad (24)$$

where as last step we inserted Eq. (22) for the $N \gg 1$ limit. Comparing Eq. (23) and Eq. (24), we find that the bound is approximately saturated, demonstrating that Eq. (24) is indeed a tight bound and cannot be improved further.

5 Random Hamiltonian evolution

Next, we study the evolution of states under random Hamiltonians [6]. We evolve an initial random stabilizer state $|\psi(0)\rangle = |\psi_{\text{STAB}}\rangle$ state

$$|\psi(t)\rangle = e^{-iHt} |\psi(0)\rangle \quad (25)$$

in time t . The Hamiltonian H is chosen as a random matrix sampled from the Gaussian unitary ensemble (GUE).

We now calculate the SRE for the evolution with the random Hamiltonians. First, we define the fidelity F with the initial stabilizer state

$$F = |\langle \psi(0) | \psi(t) \rangle|^2 \quad (26)$$

For $t \ll 1$, we find up to second order in t

$$F(t) \approx |\langle \psi | 1 - iHt - \frac{1}{2} H^2 t^2 | \psi \rangle|^2 \approx 1 - t^2 (\langle \psi | H^2 | \psi \rangle - \langle \psi | H | \psi \rangle^2)$$

We now normalize H such that $\langle \psi | H^2 | \psi \rangle - \langle \psi | H | \psi \rangle^2 = 1$ on average for $|\psi\rangle$ chosen from 2-designs, which is achieved by demanding that on average one has $\text{tr}(H^2) = 2^N + 1$. This normalization factor can be computed exactly via the fact that 2-designs have on average $\langle \psi | H^2 | \psi \rangle = \frac{\text{tr}(H^2)}{2^N}$ and $\langle \psi | H | \psi \rangle^2 = \frac{\text{tr}(H^2)}{2^N(2^N+1)}$. This restricts the eigenvalue spectrum of H within $[-2, 2]$ independent of N . This leads to an N -independent growth of correlations as proposed in Ref. [6].

With this normalization of H , we get on average for short times $t \ll 1$

$$F(t) \approx 1 - t^2. \quad (27)$$

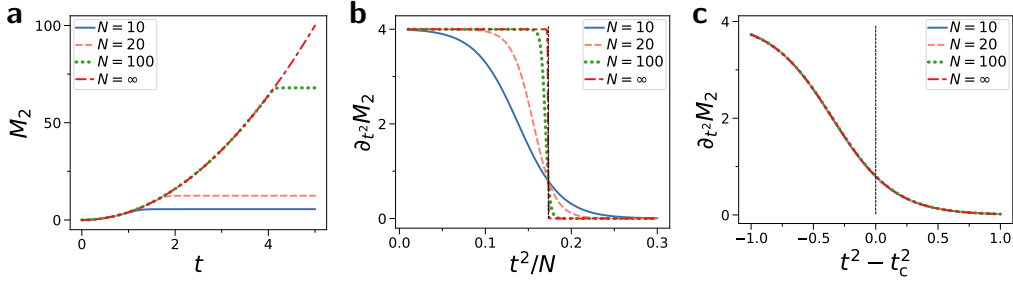


Figure 4: Universal behavior of 2-SRE for random basis evolution model Eq. (19). **a)** M_2 against time t for different N . **b)** Derivative in respect to t^2 of SRE $\partial_{t^2} M_2$ against t . Black vertical dashed line is critical time $t_c^2 = \frac{1}{4} N \ln(2)$. **c)** $\partial_{t^2} M_2$ against t^2 shifted by t_c^2 . Hallmark of universality is the crossing of all curves at the critical point t_c^2 and collapse to a single curve.

Due to Levy's lemma, observed expectation values such as $F(t)$ concentrate with exponentially high probability around its average for each sampled state [41].

Approximation of Pauli distribution. We now want to find an approximation for $M_\alpha(t)$ as function of time t . For this, we need to understand the distribution of expectation values $\beta_\sigma(t) \equiv \beta_\sigma = \langle \psi(t) | \sigma | \psi(t) \rangle$ of $|\psi(t)\rangle$. The distribution $\beta_\sigma^2 = \langle \psi | \sigma | \psi \rangle^2$ is the Pauli spectrum, i.e. the distribution of the square of Pauli string expectation values. In total, there are 4^N Pauli strings σ . Any state can be written as $\rho = 2^{-N} \sum_\sigma \beta_\sigma \sigma$, where $2^{-N} \sum_\sigma \beta_\sigma^2 = 1$ for pure states.

We have an initial stabilizer state $|\psi(0)\rangle$, which is stabilized by a commuting subgroup G of $|G| = 2^N$ Pauli strings. For any $\sigma \in G$, we have $\beta_\sigma^2 = 1$. In contrast, for $\sigma' \notin G$ we have $\beta_{\sigma'}^2 = 0$, where the complement of G contains $4^N - 2^N$ Pauli strings.

Now, how does the Pauli spectrum $\beta_\sigma(t)^2$ change when the stabilizer state is evolved in time t ? For $t = 0$, the Pauli spectrum has two peaks at $\beta_\sigma^2 = 0$ and $\beta_\sigma^2 = 1$. For $t > 0$, the two peaks shift and diffuse. However, we observe numerically that the two peaks remain highly concentrated even for relatively large t . Note that for Haar random states, the concentration has been proven [46]. We show the histogram of the Pauli spectrum in Fig. 5a. Note that up to $t \lesssim 1$, there are two distinct peaks with a gap in between them. Note that Fig. 5a is a logarithmic plot, and the peak for small β_σ^2 appears broad in logarithmic space, but is actually very concentrated close to its mean value. Let us now approximate the two peaks as Delta-functions centered around their mean value. For many qubits $N \gg 1$, we can easily compute the average of each peak, i.e. $\beta_{\sigma \in G}^2 \approx F^2$, and $\beta_{\sigma \notin G}^2 \approx 2^{-N}(1 - F^2)$.

With decreasing F , the gap between $\beta_{\sigma \notin G}^2$ and $\beta_{\sigma \in G}^2$ decreases, and the two distributions merge when $F(t)^2 \lesssim 2^{-N}$. As we will find, this happens at the critical time. We confirm numerically that different instances of H sampled from the GUE show similar spectrum.

SRE of random evolution. We now approximate the

Pauli spectrum of $|\psi(t)\rangle$ by its two observed mean values. First, we split M_α into its contribution stemming from Pauli strings in $\sigma \in G$ and $\sigma \notin G$.

$$M_\alpha = (1 - \alpha)^{-1} \ln(2^{-N} \sum_\sigma |\beta_\sigma|^{2\alpha}) = (1 - \alpha)^{-1} \ln(2^{-N} [\sum_{\sigma \in G} |\beta_\sigma|^{2\alpha} + \sum_{\sigma \notin G} |\beta_\sigma|^{2\alpha}])$$

Next, we approximate $\beta_{\sigma \in G}^2 = F^2$ and $\beta_{\sigma \notin G}^2 = 2^{-N}(1 - F^2)$ and use that $|G| = 2^N$ and $|\bar{G}| = 4^N - 2^N \approx 4^N$ for $N \gg 1$, yielding our main approximation for the SRE

$$M_\alpha(F) \approx (1 - \alpha)^{-1} \ln(F^{2\alpha} + 2^{N(1-\alpha)}(1 - F^2)) \quad (28)$$

Now, we regard the limit of $t \ll 1$ and $N \gg 1$. Here, we apply the first order Taylor expansions $F(t) \approx 1 - t^2$, $1 - F(t)^2 \approx 2t^2$ and $\ln(F(t)) \approx -t^2$ and insert them into Eq. (28).

First, we study $\alpha < 1$. We first demand that $2^{N(1-\alpha)}(1 - F^2)^\alpha \ll 1$ or $t \ll \frac{1}{\sqrt{2}} 2^{-N(1-\alpha)/(2\alpha)}$, i.e. exponentially small times

$$M_{\alpha < 1} \approx (1 - \alpha)^{-1} 2^{N(1-\alpha)} (1 - F^2)^\alpha \approx \frac{2^\alpha}{1 - \alpha} 2^{N(1-\alpha)} t^{2\alpha}. \quad (29)$$

The growth in $M_{\alpha < 1}$ is polynomial in t and exponential in N . Beyond exponentially small times $2^{N(1-\alpha)}(1 - F^2)^\alpha \gg 1$ and $t^2 \leq \frac{1}{2}$, we get for $\alpha < 1$

$$M_{\alpha < 1} \approx (1 - \alpha)^{-1} (N(1 - \alpha) \ln(2) + \alpha \ln(1 - F^2)) \approx \frac{\alpha}{1 - \alpha} \ln(2t^2) + N \ln(2). \quad (30)$$

In particular, for $t \sim 1/\text{poly}(N)$, we find extensive $M_{\alpha < 1} \sim N$.

Next, we regard the case $\alpha = 1$, $t^2 \leq \frac{1}{2}$ and $N \gg 1$. Here, we have

$$M_1 = 2^{-N} \sum_\sigma \beta_\sigma^2 \ln(\beta_\sigma^2) = -F^2 \ln(F^2) - (1 - F^2) \ln(2^{-N}(1 - F^2)) = 2F^2 \ln(F) + N(1 - F^2) \ln(2) - (1 - F^2) \ln(1 - F^2) \approx 2(1 - t^2)^2 t^2 + 2Nt^2 \ln(2) - 2t^2 \ln(2t^2) \approx 2t^2(N \ln(2) - \ln(2t^2)). \quad (31)$$

Finally, we study the case $\alpha > 1$, where we find

$$M_{\alpha>1} \approx (1-\alpha)^{-1} \ln(F^{2\alpha}) = \frac{2\alpha}{1-\alpha} \ln(F) \approx \frac{2\alpha}{\alpha-1} t^2. \quad (32)$$

where we highlight that the growth is independent of N . For $\alpha = 2$ we have $M_2 \approx 4t^2$, matching the result for the evolution in random bases of Eq. (22). Also note that by comparing with Eq. (6) it is easy to see that all $\alpha > 1$ provide tight lower bounds to D_{\min} .

Our analytic results match numerical simulations as shown in Fig. 5b for all investigated α and N . While we assumed small t for the approximations, we observe that our equations match our numerical studies until the critical time where the SRE becomes maximal.

Critical time. We now estimate the critical time $t_{c,\alpha}$ for evolution with random Hamiltonians using our approximation. While these equations were derived for the limit of small t , our numeric suggest that the approximations work well up to the critical time when the SRE becomes maximal. We define the critical time $t_{c,\alpha}$ as the time when the SRE converges to its maximal value, i.e. $M_\alpha(t_{c,\alpha}) = M_\alpha^{\max}$, where M_α^{\max} has been computed in Eq. (17) and we consider $N \gg 1$. We now study $t_{c,\alpha}$ for different α and its scaling with N .

First, SRE for $\alpha = 0$ as given by Eq. (14) relates to the number of Pauli expectation values which are exactly zero. The GUE evolution evolves all elements of the Pauli spectrum non-trivially and makes them non-zero with overwhelming probability, thus we get $\langle \psi(t) | \sigma | \psi(t) \rangle^2 \neq 0$ for $\sigma \in \mathcal{P}$ for any $t > 0$. Thus, the critical time is at

$$t_{c,0} = 0, \quad (33)$$

matching the divergence observed in Eq. (29). Next, we study $0 < \alpha < 1$. Here, inserting Eq. (30) into $M_\alpha(t_{c,\alpha}) = M_\alpha^{\max}$ gives us

$$t_{c,\alpha}^2 \approx \frac{1}{2}. \quad (34)$$

Most importantly, we find that the critical time is independent of N .

Finally, for $\alpha > 1$ we find using Eq. (32) that the critical time grows linearly in N

$$\begin{aligned} 1 < \alpha \leq 2: \quad t_{c,\alpha}^2 &\approx -\frac{1-\alpha}{2\alpha} N \ln(2), \\ \alpha > 2: \quad t_{c,\alpha}^2 &\approx \frac{1}{2\alpha} N \ln(2). \end{aligned} \quad (35)$$

Note that there may be constant corrections to t_c not captured by our first-order approximations. However, we argue that the scaling of t_c with N is accurately captured by our approximations, as we get a good match between our derived formulas and numerical studies. Our approximations were derived with the first order approximation of the fidelity $F \sim 1 - t^2$.

We numerically study the behavior of F for larger t . We find $F \sim e^{-t^2}$ up to a time $t \sim \sqrt{N}$. When inserting $F \sim e^{-t^2}$ into Eq. (28), we also get Eq. (32), indicating that Eq. (32) is indeed valid up to $t \sim \sqrt{N}$. We note that at $\alpha = 1$ a transition from constant to linear scaling occurs. We believe logarithmic corrections could appear here, however this warrants further studies.

Finally, as we show in Appendix A, the Pauli spectrum and SRE of the GUE evolution matches closely the dynamics of the random basis evolution of Sec. 4. We also observe that the SREs for both models match. Thus, we argue that the scale-invariant behavior that we shown analytically in Sec. 4 for random bases evolution also emerges for the evolution with random Hamiltonians.

6 Complexity and SRE

We now show that SREs can be related to the complexity of different operational tasks, where the type of task depends on α . In particular, we relate $\alpha > 1$ to approximate fidelity estimation, while $\alpha < 1$ to Clifford simulation complexity.

First, we note that for $\alpha > 1$, the SRE is similar to D_{\min} , which is the distance to the closest stabilizer state [22]. We find that the previously proven lower bound [20] is indeed tight for random evolutions Eq. (24) which we numerically confirm in Appendix C. Note that numeric evidence shows that SREs for $\alpha > 1$ also provide an N -independent upper bound to D_{\min} [22]. As such, we argue that SREs with $\alpha > 1$ probe the closeness to the nearest stabilizer state.

SREs with $\alpha = 2$ have been shown an explicit operational meaning: They give a lower bound on fidelity estimation [8, 30]: Given a target state $|\psi\rangle$, one can estimate the fidelity with actual state ρ by measuring Pauli expectation values [8]. The number of samples m to estimate the fidelity is lower bounded as $m \gtrsim \exp(M_2(|\psi\rangle))$, while an upper bound is given by $m \lesssim \exp(M_0(|\psi\rangle))$ [30].

In Appendix D, we show an explicit fidelity estimation algorithm whose efficiency is directly given by $M_2(|\psi\rangle)$: First, we note that fidelity estimation works especially well when $|\psi\rangle$ is a stabilizer state. Now, if $|\psi\rangle$ is not a stabilizer, but close to stabilizer state, then one can use this stabilizer state as a proxy for fidelity estimation: One estimates the fidelity of ρ with the closest stabilizer state $\arg\max_{|\psi_{\text{STAB}}\rangle} |\langle \psi | \psi_{\text{STAB}} \rangle|^2$. We show that when $|\psi\rangle$ is close to a stabilizer state, this is a good approximation of the fidelity, where the quality depends on $M_2(|\psi\rangle)$. In particular, we show in Appendix D that this scheme has an error $\Delta F \leq 2\sqrt{1 - \exp(-M_2(|\psi\rangle))}$ and gives a non-trivial approximation of the fidelity as long as $M_2(|\psi\rangle) \leq \log(4/3)$.

In contrast, SREs with $\alpha < 1$ (especially $\alpha = 1/2$)

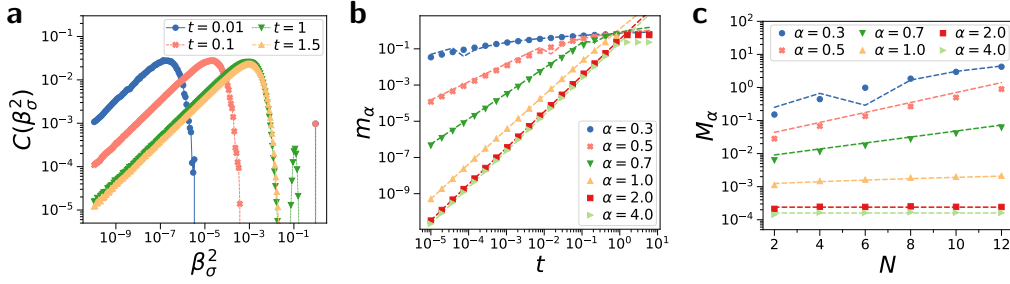


Figure 5: α -SREs of random Hamiltonian evolution. **a)** Pauli spectrum plotted as histogram, where we show the probability C of observing the Pauli expectation values $\beta_\sigma^2 = \langle \psi | \sigma | \psi \rangle^2$. We show different t of GUE evolution for $N = 10$ and averages over 20 random instances. For clarity, we do not show the trivial identity operator $\langle \psi | I | \psi \rangle^2 = 1$ of the spectrum. **b)** SRE density m , where dashed lines are approximations Eq. (32), Eq. (29), Eq. (30) and Eq. (31). The sudden change of the dashed line for $\alpha < 1$ is due to the change from Eq. (29) to Eq. (30) at $2^{N(1-\alpha)}(1 - F^2)^\alpha = 1$. **c)** SRE M against N for $t = 10^{-2}$. Dashed line is fit with approximations. Our model accurately describes α -SREs of random evolution as function of N and t , allowing us to predict overall scaling and critical time $t_{c,\alpha}$.

show behavior similar to the log-free robustness of magic LR [24, 33, 42] or max-relative entropy of magic [4, 33]. They respectively relate to the negativity of the mixture of stabilizer states, or the number of superpositions of stabilizer states needed to represent a given state. LR has been used to estimate fault-tolerant state preparation complexity and relates to the complexity of Clifford based simulation algorithms. These algorithms simulate quantum circuits as Clifford circuits injected with nonstabilizer gates, where the simulation complexity commonly increase exponentially with the number of nonstabilizer gates [3]. In fact, $M_{1/2}$ has been used as a proxy for LR to evaluate simulation complexity of Clifford-based simulation algorithms [42]. Further, we find that the lower bound $\text{LR} \geq \frac{1}{2}M_{1/2}$ Eq. (8) is tight for random evolution (see Appendix C). Additionally, M_0 is a lower bound to the stabilizer nullity $\nu \geq M_0$, which characterizes the complexity of Clifford-based learning algorithms [11, 14, 17, 32].

SRE dynamics and complexity. Now, we study the complexity of different tasks for doped Clifford circuits and random evolution using SREs.

For Clifford gates injected with T-gates, SREs converge for all α to their maximum $M_\alpha \sim N$ at T-gate density $q \sim \text{const}$. This is because each T-gate affects only a discrete subset of the Pauli spectrum. We numerically find that D_{\min} and LR appear to show this behavior as well. This implies that fidelity with the closest stabilizer state and classical cost of simulation with Clifford+T correlate. In particular, for $q \sim 1/N$ and thus $M_\alpha = \text{const}$, one can efficiently simulate and learn the state [11, 17, 32], as well as estimate the fidelity [30]. In contrast, for $q \sim \text{const}$ and thus $M_\alpha \sim N$ simulation, learning and fidelity estimation is unlikely to be efficient [2, 3, 28].

In contrast, SREs for random evolution shows widely different behavior depending on α . This is because random evolution affects all Pauli strings even at short evolution times. For $\alpha > 1$, $M_{\alpha>1}$ grows as

$\propto t^2$ and converges to its maximum at $t_{c,\alpha>1} \sim \sqrt{N}$. For $t = \text{const}$, we have $M_{\alpha>1} = \text{const}$ and $D_{\min} = \text{const}$, i.e. the evolution is close to a stabilizer state in terms of fidelity. Thus, at $t = \text{const}$ one can efficiently certify the fidelity of random evolution (see Appendix D).

$\alpha < 1$ shows a completely different behavior, growing extremely fast with t : For $\alpha = 0$, M_0 is maximal for any $t > 0$, which implies that stabilizer nullity ν is maximal, rendering known near-Clifford learning algorithms inefficient [11, 17, 32]. For $0 < \alpha < 1$, SREs saturate rapidly at constant evolution time $t_{c,0<\alpha<1} \approx \frac{1}{2}$. Further, extensive $M_{\alpha<1} \sim N$ is reached already for $t \gtrsim 1/\text{poly}(N)$. This hints that simulating random dynamics to arbitrary precision with Clifford simulation algorithms becomes classically intractable already at $t \gtrsim 1/\text{poly}(N)$.

We summarize the growth of SRE for random Hamiltonian evolution with time t , and circuits composed of Clifford unitaries and T-gates with T-gate density q in Fig. 6. In particular, we highlight the extremely fast growth in time t for random evolution for $\alpha < 1$, which is not observed for $\alpha > 1$ or for Clifford+T circuits for any α .

Finally, we note that the complexity of tasks related to entanglement tasks can be bounded using the stabilizer nullity [14]. For small stabilizer nullity, one can efficiently do entanglement estimation, distillation and dilution. The same tasks become hard when the stabilizer nullity becomes extensive. For Cliffords doped with a constant number of T-gates we have a constant stabilizer nullity, and thus entanglement-related tasks are easy. In contrast, for random evolution the stabilizer nullity becomes already maximal for exponentially small times, where entanglement-related tasks become hard.

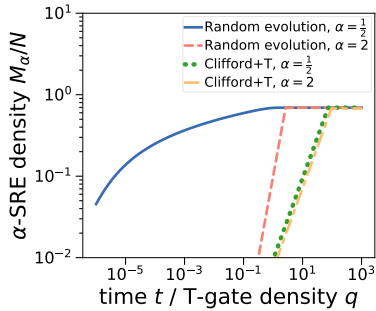


Figure 6: SRE of random Hamiltonian evolution for $\alpha < 1$ increases extremely fast with time t . In contrast, for $\alpha > 1$, as well as Clifford + T circuits for any α , the growth in SRE is much slower. We show SRE density M_α/N for random Hamiltonian evolution with Eq. (28) and doped Clifford circuits with Eq. (15) for $N = 40$.

7 Discussion

We have studied α -SREs for random Clifford circuits doped with T-gates and random time evolution where we demonstrated the connection of Rényi index α to different aspects of complexity of quantum states.

We find that the SRE converges to the maximum at a critical T-gate density $q_{c,\alpha}$ and time $t_{c,\alpha}$ in the thermodynamic limit. We determine the transition exactly for $\alpha = 2$, while for general α we determine the convergence using heuristic models of the Pauli spectrum. For $\alpha = 2$, we observe universal behavior around the critical point where the derivative of the SRE can be rescaled onto a single curve for all N . This hints that the saturation transition is connected to phase transitions, where universal behavior is commonly found, for example for the transition between different phases of quantum many-body system [39] or at complexity transitions in classical and quantum algorithms [50].

The critical T-gate density $q_{c,\alpha}$ shows non-monotonous behavior as function of Rényi index α , and the critical evolution time $t_{c,\alpha}$ even changes its scaling with qubit number N . This behavior highlights the fact that SREs with different α , i.e. different moments of the Pauli spectrum $\langle \psi | \sigma | \psi \rangle^{2\alpha}$, probe different aspects of nonstabilizerness.

SREs with $\alpha < 1$ and $\alpha > 1$ probe two different aspects of nonstabilizerness: We find that SREs with $\alpha < 1$ behave similar to the log-free robustness of magic LR [24, 33, 42] or max-relative entropy of magic [4, 33]. Roughly, these magic monotones relate to the complexity of approximating a state using a superposition of stabilizer states. In contrast, $\alpha > 1$ SREs can be related [22] to the min-relative entropy of magic D_{\min} [4, 33], which measure the fidelity with the closest stabilizer state.

We find that random Hamiltonian evolution has a fundamental separation in nonstabilizerness complexity: Simulating random evolution using Clifford-based

algorithms to arbitrary precision is already hard for very small times $t \gtrsim 1/\text{poly}(N)$. In contrast, up to $t = \text{const}$ one can efficiently certify the fidelity of the evolved state within some fixed error $\Delta F \approx 4t$. We show the algorithm in Appendix D by certifying in respect to a stabilizer approximation of the state. In contrast, for Cliffords doped with T-gates, simulation and certification complexity correlate, and become intractable for the same T-gate density $q \gtrsim \log(N)$.

Finally, for both random evolution and Clifford+T model, the critical time and T-gate density is maximal for $\alpha = 2$. This indicates that the 2-SRE holds a special status. Coincidentally, for $\alpha < 2$, the SRE is known not to be a monotone [20], while for $\alpha \geq 2$ it is a pure state monotone [27].

Finally, we want to highlight the technical contributions of our work which may be of independent interest: We show heuristically that the Pauli spectrum of random Hamiltonian evolution can be approximated by two distinct peaks. With increasing time, the two peaks shift towards each other and eventually merge. This is exactly when the SRE becomes maximal. At last, we introduce a class of random evolution in Eq. (19), which can be seen as evolution in random Clifford bases. This evolution behaves very similar to random Hamiltonian evolution, where we observe numerically the same Pauli spectrum. It can be expressed as random Clifford circuits combined with small-angle single-qubit rotations. This allows us to compute its 2-SRE analytically for all times t . The random Clifford bases evolution could serve as a model of random evolution with an exact circuit representation.

Acknowledgements

We thank Hyukjoon Kwon, Ludovico Lami and especially Lorenzo Piroli for inspiring discussions. This work is supported by a Samsung GRC project and the UK Hub in Quantum Computing and Simulation, part of the UK National Quantum Technologies Programme with funding from UKRI EPSRC grant EP/T001062/1.

References

- [1] Dolev Bluvstein, Harry Levine, Giulia Semeghini, Tout T Wang, Sepehr Ebadi, Marcin Kalinowski, Alexander Keesling, Nishad Maskara, Hannes Pichler, Markus Greiner, et al. A quantum processor based on coherent transport of entangled atom arrays. *Nature*, 604(7906):451–456, 2022.
- [2] Sergey Bravyi and David Gosset. Improved classical simulation of quantum circuits dominated by clifford gates. *Phys. Rev. Lett.*, 116:250501, Jun 2016. DOI: [10.1103/PhysRevLett.116.250501](https://doi.org/10.1103/PhysRevLett.116.250501)

- RevLett.116.250501. URL <https://link.aps.org/doi/10.1103/PhysRevLett.116.250501>.
- [3] Sergey Bravyi, Graeme Smith, and John A. Smolin. Trading classical and quantum computational resources. *Phys. Rev. X*, 6: 021043, Jun 2016. DOI: [10.1103/PhysRevX.6.021043](https://doi.org/10.1103/PhysRevX.6.021043). URL <https://link.aps.org/doi/10.1103/PhysRevX.6.021043>.
- [4] Sergey Bravyi, Dan Browne, Padraic Calpin, Earl Campbell, David Gosset, and Mark Howard. Simulation of quantum circuits by low-rank stabilizer decompositions. *Quantum*, 3:181, 2019. DOI: [10.22331/q-2019-09-02-181](https://doi.org/10.22331/q-2019-09-02-181). URL <https://quantum-journal.org/papers/q-2019-09-02-181/>.
- [5] Raphael Brieger, Markus Heinrich, Ingo Roth, and Martin Kliesch. Stability of classical shadows under gate-dependent noise. *arXiv:2310.19947*, 2023.
- [6] Jordan Cotler, Nicholas Hunter-Jones, Junyu Liu, and Beni Yoshida. Chaos, complexity, and random matrices. *Journal of High Energy Physics*, 2017(11):1–60, 2017.
- [7] Tyler D Ellison, Kohtaro Kato, Zi-Wen Liu, and Timothy H Hsieh. Symmetry-protected sign problem and magic in quantum phases of matter. *Quantum*, 5:612, 2021. DOI: [10.22331/q-2021-12-28-612](https://doi.org/10.22331/q-2021-12-28-612). URL <https://quantum-journal.org/papers/q-2021-12-28-612/>.
- [8] Steven T Flammia and Yi-Kai Liu. Direct fidelity estimation from few pauli measurements. *Physical review letters*, 106(23):230501, 2011.
- [9] M Frau, PS Tarabunga, M Collura, M Dalmonde, and E Tirrito. Non-stabilizerness versus entanglement in matrix product states. *arXiv:2404.18768*, 2024.
- [10] Roy J Garcia, Kaifeng Bu, and Arthur Jaffe. Resource theory of quantum scrambling. *Proceedings of the National Academy of Sciences*, 120(17):e2217031120, 2023.
- [11] Sabee Grewal, Vishnu Iyer, William Kretschmer, and Daniel Liang. Efficient learning of quantum states prepared with few non-clifford gates. *arXiv:2305.13409*, 2023.
- [12] Andi Gu, Lorenzo Leone, Soumik Ghosh, Jens Eisert, Susanne F Yelin, and Yihui Quek. Pseudomagic quantum states. *Physical Review Letters*, 132(21):210602, 2024.
- [13] Andi Gu, Salvatore FE Oliviero, and Lorenzo Leone. Doped stabilizer states in many-body physics and where to find them. *arXiv:2403.14912*, 2024.
- [14] Andi Gu, Salvatore FE Oliviero, and Lorenzo Leone. Magic-induced computational separation in entanglement theory. *arXiv preprint arXiv:2403.19610*, 2024.
- [15] Jeongwan Haah, Yunchao Liu, and Xinyu Tan. Efficient approximate unitary designs from random pauli rotations. *arXiv preprint arXiv:2402.05239*, 2024.
- [16] J Haferkamp, F Montealegre-Mora, M Heinrich, J Eisert, D Gross, and I Roth. Efficient unitary designs with a system-size independent number of non-clifford gates. *Communications in Mathematical Physics*, pages 1–47, 2022.
- [17] Dominik Hangleiter and Michael J Gullans. Bell sampling from quantum circuits. *arXiv:2306.00083*, 2023.
- [18] Tobias Haug and M.S. Kim. Scalable measures of magic resource for quantum computers. *PRX Quantum*, 4:010301, Jan 2023. DOI: [10.1103/PRXQuantum.4.010301](https://doi.org/10.1103/PRXQuantum.4.010301). URL <https://link.aps.org/doi/10.1103/PRXQuantum.4.010301>.
- [19] Tobias Haug and Lorenzo Piroli. Quantifying nonstabilizerness of matrix product states. *Phys. Rev. B*, 107(3):035148, 2023. DOI: [10.1103/PhysRevB.107.035148](https://doi.org/10.1103/PhysRevB.107.035148). URL <https://link.aps.org/doi/10.1103/PhysRevB.107.035148>.
- [20] Tobias Haug and Lorenzo Piroli. Stabilizer entropies and nonstabilizerness monotones. *Quantum*, 7:1092, 2023.
- [21] Tobias Haug, Kishor Bharti, and Dax Enshan Koh. Pseudorandom unitaries are neither real nor sparse nor noise-robust. *arXiv:2306.11677*, 2023.
- [22] Tobias Haug, Soovin Lee, and M. S. Kim. Efficient quantum algorithms for stabilizer entropies. *Phys. Rev. Lett.*, 132:240602, Jun 2024. DOI: [10.1103/PhysRevLett.132.240602](https://doi.org/10.1103/PhysRevLett.132.240602). URL <https://link.aps.org/doi/10.1103/PhysRevLett.132.240602>.
- [23] Marcel Hinsche, Marios Ioannou, Sofiene Jerbi, Lorenzo Leone, Jens Eisert, and Jose Carrasco. Efficient distributed inner product estimation via pauli sampling. *arXiv:2405.06544*, 2024.
- [24] Mark Howard and Earl Campbell. Application of a resource theory for magic states to fault-tolerant quantum computing. *Phys. Rev. Lett.*, 118:090501, Mar 2017. DOI: [10.1103/PhysRevLett.118.090501](https://doi.org/10.1103/PhysRevLett.118.090501). URL <https://link.aps.org/doi/10.1103/PhysRevLett.118.090501>.
- [25] Guglielmo Lami and Mario Collura. Non-stabilizerness via perfect pauli sampling of matrix product states. *Phys. Rev. Lett.*, 131:180401, Oct 2023. DOI: [10.1103/PhysRevLett.131.180401](https://doi.org/10.1103/PhysRevLett.131.180401). URL <https://link.aps.org/doi/10.1103/PhysRevLett.131.180401>.
- [26] Guglielmo Lami, Tobias Haug, and Jacopo De Nardis. Quantum state designs with clifford enhanced matrix product states. *arXiv:2404.18751*, 2024.
- [27] Lorenzo Leone and Lennart Bittel. Stabilizer entropies are monotones for magic-state resource theory. *arXiv:2404.11652*, 2024.
- [28] Lorenzo Leone, Salvatore F. E. Oliviero, You

- Zhou, and Alioscia Hamma. Quantum chaos is quantum. *Quantum*, 5:453, 2021. URL <https://arxiv.org/abs/2102.08406>.
- [29] Lorenzo Leone, Salvatore F. E. Oliviero, and Alioscia Hamma. Stabilizer rényi entropy. *Phys. Rev. Lett.*, 128:050402, Feb 2022. DOI: [10.1103/PhysRevLett.128.050402](https://doi.org/10.1103/PhysRevLett.128.050402). URL <https://link.aps.org/doi/10.1103/PhysRevLett.128.050402>.
- [30] Lorenzo Leone, Salvatore F. E. Oliviero, and Alioscia Hamma. Nonstabilizerness determining the hardness of direct fidelity estimation. *Phys. Rev. A*, 107:022429, Feb 2023. DOI: [10.1103/PhysRevA.107.022429](https://doi.org/10.1103/PhysRevA.107.022429). URL <https://link.aps.org/doi/10.1103/PhysRevA.107.022429>.
- [31] Lorenzo Leone, Salvatore FE Oliviero, Gianluca Esposito, and Alioscia Hamma. Phase transition in stabilizer entropy and efficient purity estimation. *Physical Review A*, 109(3):032403, 2024.
- [32] Lorenzo Leone, Salvatore FE Oliviero, and Alioscia Hamma. Learning t-doped stabilizer states. *Quantum*, 8:1361, 2024.
- [33] Zi-Wen Liu and Andreas Winter. Many-body quantum magic. *PRX Quantum*, 3:020333, May 2022. DOI: [10.1103/PRXQuantum.3.020333](https://doi.org/10.1103/PRXQuantum.3.020333). URL <https://link.aps.org/doi/10.1103/PRXQuantum.3.020333>.
- [34] Jordi Arnau Montaña López and Pavel Kos. Exact solution of long-range stabilizer rényi entropy in the dual-unitary xxz model. *arXiv:2405.04448*, 2024.
- [35] Antonio Francesco Mello, Alessandro Santini, and Mario Collura. Hybrid stabilizer matrix product operator. *arXiv:2405.06045*, 2024.
- [36] Pradeep Niroula, Christopher David White, Qingfeng Wang, Sonika Johri, Daiwei Zhu, Christopher Monroe, Crystal Noel, and Michael J. Gullans. Phase transition in magic with random quantum circuits. *arXiv:2304.10481*, 2023.
- [37] Jovan Odavić, Tobias Haug, Gianpaolo Torre, Alioscia Hamma, Fabio Franchini, and Salvatore Marco Giampaolo. Complexity of frustration: A new source of non-local non-stabilizerness. *SciPost Physics*, 15(4):131, 2023.
- [38] Salvatore F. E. Oliviero, Lorenzo Leone, Alioscia Hamma, and Seth Lloyd. Measuring magic on a quantum processor. *npj Quantum Information*, 8(1):148, 2022. DOI: [10.1038/s41534-022-00666-5](https://doi.org/10.1038/s41534-022-00666-5).
- [39] Andreas Osterloh, Luigi Amico, Giuseppe Falci, and Rosario Fazio. Scaling of entanglement close to a quantum phase transition. *Nature*, 416(6881):608–610, 2002. DOI: [10.1038/416608a](https://doi.org/10.1038/416608a). URL <https://www.nature.com/articles/416608a>.
- [40] Alessio Paviglianiti, Guglielmo Lami, Mario Collura, and Alessandro Silva. Estimating non-stabilizerness dynamics without simulating it. *arXiv:2405.06054*, 2024.
- [41] Sandu Popescu, Anthony J Short, and Andreas Winter. Entanglement and the foundations of statistical mechanics. *Nature Physics*, 2(11):754–758, 2006. DOI: [10.1038/nphys444](https://doi.org/10.1038/nphys444).
- [42] Patrick Rall, Daniel Liang, Jeremy Cook, and William Kretschmer. Simulation of qubit quantum circuits via pauli propagation. *Phys. Rev. A*, 99:062337, Jun 2019. DOI: [10.1103/PhysRevA.99.062337](https://doi.org/10.1103/PhysRevA.99.062337). URL <https://link.aps.org/doi/10.1103/PhysRevA.99.062337>.
- [43] Saubhik Sarkar, Chiranjib Mukhopadhyay, and Abolfazl Bayat. Characterization of an operational quantum resource in a critical many-body system. *New J. Phys.*, 22(8):083077, 2020. DOI: [10.1088/1367-2630/aba919](https://doi.org/10.1088/1367-2630/aba919). URL <https://iopscience.iop.org/article/10.1088/1367-2630/aba919>.
- [44] Poetri Sonya Tarabunga, Emanuele Tirrito, Titas Chanda, and Marcello Dalmonte. Many-body magic via pauli-markov chains—from criticality to gauge theories. *PRX Quantum*, 4(4):040317, 2023.
- [45] Emanuele Tirrito, Poetri Sonya Tarabunga, Guglielmo Lami, Titas Chanda, Lorenzo Leone, Salvatore FE Oliviero, Marcello Dalmonte, Mario Collura, and Alioscia Hamma. Quantifying non-stabilizerness through entanglement spectrum flatness. *Physical Review A*, 109(4):L040401, 2024.
- [46] Xhek Turkeshi, Anatoly Dymarsky, and Piotr Sierant. Pauli spectrum and magic of typical quantum many-body states. *arXiv:2312.11631*, 2023.
- [47] Xhek Turkeshi, Marco Schirò, and Piotr Sierant. Measuring nonstabilizerness via multifractal flatness. *Physical Review A*, 108(4):042408, 2023.
- [48] Victor Veitch, SA Hamed Mousavian, Daniel Gottesman, and Joseph Emerson. The resource theory of stabilizer quantum computation. *New J. Phys.*, 16(1):013009, 2014. URL <https://doi.org/10.1088/1367-2630/16/1/013009>.
- [49] Christopher David White, ChunJun Cao, and Brian Swingle. Conformal field theories are magical. *Phys. Rev. B*, 103:075145, Feb 2021. DOI: [10.1103/PhysRevB.103.075145](https://doi.org/10.1103/PhysRevB.103.075145). URL <https://link.aps.org/doi/10.1103/PhysRevB.103.075145>.
- [50] Bingzhi Zhang, Akira Sone, and Quntao Zhuang. Quantum computational phase transition in combinatorial problems. *npj Quantum Information*, 8(1):87, 2022.

Appendix

We provide additional technical details and data supporting the claims in the main text.

A GUE evolution and random basis evolution

We now give numeric evidence that the evolution via $|\psi(t)\rangle = \exp(-iHt)|0\rangle$ with a random Hamiltonian H sampled from the GUE has on average the same Pauli spectrum as the evolution in random Clifford bases via $d \gg N$ single-qubit rotations with parameters $\theta = 2t/\sqrt{d}$ as defined in Eq. (19).

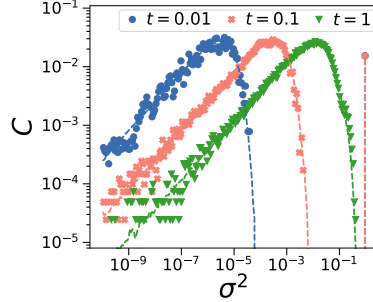


Figure S1: Pauli spectrum plotted as histogram over occurrences C of observing Pauli expectation value $\langle \sigma \rangle^2$. The dots for evolution in random Clifford bases with rotations $\theta = 2t/\sqrt{d}$ for different t . The dashed line is evolution with GUE Hamiltonian. We show $N = 6$, $d = 1000$ and average over 1000 random Hamiltonians and 10 circuits. For clarity, we do not show the trivial identity operator $\langle \psi | I | \psi \rangle^2 = 1$ of the spectrum.

In Fig. S1, we plot the Pauli spectrum, where $C(\langle \psi | \sigma | \psi \rangle^2)$ is the probability of finding Pauli expectation value $\langle \psi | \sigma | \psi \rangle^2$ of Pauli σ for a given state $|\psi(t)\rangle$. We show $C(\langle \psi | \sigma | \psi \rangle^2)$ for different t for evolution in random Clifford bases (dots) as well as the GUE evolution with same t (dashed lines). We observe that both match nearly perfectly, indicating that they have the same statistical properties in terms of Pauli spectrum and SRE.

While we believe that both evolutions show similar behavior for polynomial times, we note that for very long times (on the scale of $t \sim 2^{N/2}$) both models likely show different behavior in terms of deep thermalization [6], as the GUE Hamiltonian evolution conserves energy while the other model does not. It has been noted that the ensemble of GUE evolutions forms an exact k -design at polynomial times, however stops being a k -design at exponential times. This behavior at long times is attributed to energy conservation of the evolution, which at long times leads to a dephasing due to the energy eigenvalues. For non-energy conserved dynamics this behavior at long times is not expected. However, this difference at exponential times is evident in the k -design properties, however it may not be evident in the Pauli spectrum and SRE [22].

The study of this subtleties at exponential times is difficult numerically, and we leave a formal study of the statistical similarity between Eq. (19) and evolution with random Hamiltonians as an open problem.

B Min-relative entropy of magic scaling for random evolution

We show the min-relative entropy of magic D_{\min} as function of time t for evolution with random Hamiltonians sampled from the GUE. We find that the increase with t can be approximated by $D_{\min} \approx t^2$ up to the time when it converges to its maximal value $D_{\min} \leq N \ln(2)$.

C SRE, min-relative entropy and robustness

Here, we study the relationship between α -SREs, min-relative entropy D_{\min} and log-free robustness LR. We show in Fig. S3a the growth of M_α , min-relative entropy D_{\min} and log-free robustness LR with N_T . Here, we rescaled D_{\min} and LR such that they correspond to their respective bounds, i.e. $2LR \geq M_{1/2}$ and $4D_{\min} \geq M_2$. In Fig. S3a, we show the Clifford-T circuit, we find that M_α is indeed is a lower bound, which is non-tight. In Fig. S3b, we show evolution with random Hamiltonian. Here, the lower bounds match closely, indicating that they are indeed tight. We also note the relationship between LR, D_{\min} and α . For $\alpha < 1$, LR and M_α show similar growth, indicating that they relate to classical simulation complexity. While for $\alpha > 1$, M_α growth rate is similar to D_{\min} which measures the distance to the closest stabilizer state. We also note that the convergence

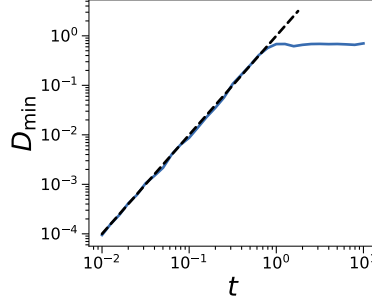


Figure S2: Min-relative entropy of magic D_{\min} as function of t for evolution with GUE Hamiltonian. Dashed line is t^2 . We show $N = 4$.

to maximal M_α shows completely different scaling depending on α , with $t_{c,\alpha < 1}^2 = \text{const}$, while $t_{c,\alpha > 1}^2 \propto N$. Note that this behavior is difficult to see for small N .

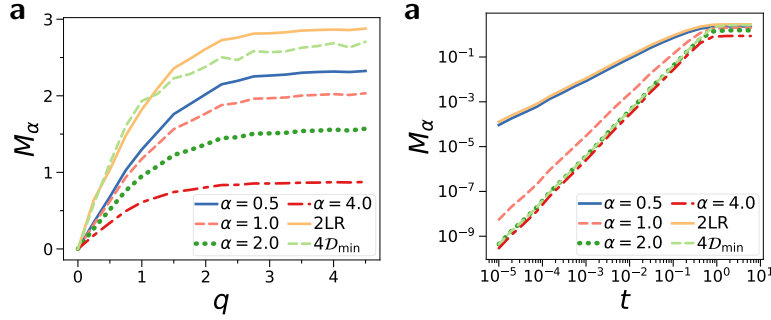


Figure S3: Relationship of α -SRE with min-relative entropy D_{\min} and log-free robustness LR. Here, we rescaled D_{\min} and LR to pose lower bounds on SRE. **a)** Clifford+T circuit for $N = 4$ qubits against T-gate density q . **b)** Evolution with random Hamiltonian sampled from GUE against time t .

D State certification via Pauli measurements and SREs

A common task is state certification to check whether the prepared state ρ is close to the ideal state $|\psi\rangle$ that one actually wanted to prepare. For this task, Ref. [8] proposed a simple algorithm that only requires to measure Pauli strings of the actual state. First, note that one can decompose any state in terms of its Pauli strings, i.e. $\rho = 2^{-N} \sum_{\sigma \in \mathcal{P}} \beta_\sigma \sigma$ with Pauli expectation values $\beta_\sigma(\rho) = \text{tr}(\rho \sigma)$. The fidelity between ρ and $|\psi\rangle$ is given by

$$F(\rho, |\psi\rangle) = \langle \psi | \rho | \psi \rangle = 2^{-N} \sum_{\sigma \in \mathcal{P}} \beta_\sigma(|\psi\rangle) \beta_\sigma(\rho) \quad (\text{S1})$$

Now, we note that $P_{|\psi\rangle}(\sigma) = 2^{-N} \beta_\sigma(|\psi\rangle)^2$ is a probability distribution for any pure state $|\psi\rangle$. We can rewrite the fidelity estimation into a sampling problem

$$F(\rho, |\psi\rangle) = \sum_{\sigma \in \mathcal{P}} P(\sigma) \frac{\beta_\sigma(\rho)}{\beta_\sigma(|\psi\rangle)} = \mathbb{E}_{\sigma \sim P_{|\psi\rangle}} \left[\frac{\beta_\sigma(\rho)}{\beta_\sigma(|\psi\rangle)} \right]. \quad (\text{S2})$$

Thus, to estimate F we only need to sample from $P_{|\psi\rangle}(\sigma)$ and compute $\beta_\sigma(|\psi\rangle)$ using some classical algorithm, and then measure the Pauli expectation value $\beta_\sigma(\rho)$ of the actual state ρ on the quantum device.

One can bound the number of Pauli measurements m needed on the quantum computer using the SRE [30]:

$$\frac{2}{\epsilon^2} \ln(2/\delta) \exp(M_2(|\psi\rangle)) \geq m \geq \frac{64}{\epsilon^4} \ln(2/\delta) \exp(M_0(|\psi\rangle)) \quad (\text{S3})$$

where ϵ is the additive accuracy and δ the probability the protocol fails. Most importantly, this algorithm has no assumptions on experimental state ρ , and only depends on properties of the reference state $|\psi\rangle$. The protocol is always sample efficient when $M_0(|\psi\rangle) = O(\log(N))$. For example, stabilizer states can be certified with $O(1)$ samples.

Now, what happens for nonstabilizer states? From the lower bound, we know that the protocol becomes definitely inefficient when $M_2(|\psi\rangle) = \omega(\log(N))$. Thus, the protocol fails for the T-gate doped Clifford states for $q = \omega(\log(N))$.

The algorithm starts failing whenever one samples a σ with small, but non-zero magnitude $0 < |\beta_\sigma(|\psi\rangle)| < \gamma$ with some small threshold γ . From experiment, one estimates $\beta_\sigma(\rho)$ up to some additive error ϵ . The resulting error is rescaled with the term in the denominator $\epsilon/\beta_\sigma(|\psi\rangle)$. Thus, to keep error low, one has to estimate $\beta_\sigma(\rho)$ to high precision $\epsilon \sim \gamma$, which requires $m = 1/\gamma^2$ samples. Thus, for $\gamma \sim 2^{-N}$ this results in an exponential cost.

Ref. [8] proposed an adapted protocol where one estimates the fidelity not in respect to $|\psi\rangle$, but in respect to a slightly perturbed state $|\psi'\rangle$ which does not feature Pauli expectation values with small, non-zero magnitudes. This incurs an error

$$|F(\rho, |\psi\rangle) - F(\rho, |\psi'\rangle)| \leq \| |\psi\rangle\langle\psi| - |\psi'\rangle\langle\psi'| \|_2 = \sqrt{2}\sqrt{1 - |\langle\psi|\psi'\rangle|^2}. \quad (\text{S4})$$

A good choice for the perturbed state $|\psi'\rangle$ is the closest stabilizer state to $|\psi\rangle$. In this case, we have

$$|F(\rho, |\psi\rangle) - F(\rho, |\psi'\rangle)| \leq \sqrt{2}\sqrt{1 - F_{\text{STAB}}(|\psi\rangle)} = \sqrt{2}\sqrt{1 - \exp(-D_{\min}(|\psi\rangle))}. \quad (\text{S5})$$

where F_{STAB} is the stabilizer fidelity [4]. F_{STAB} is lower bounded by M_2 as shown in Ref. [22]

$$F_{\text{STAB}} \geq 2 \exp(-M_2) - 1. \quad (\text{S6})$$

Thus, we get

$$\Delta F = |F(\rho, |\psi\rangle) - F(\rho, |\psi'\rangle)| \leq 2\sqrt{1 - \exp(-M_2(|\psi\rangle))}. \quad (\text{S7})$$

There is a unique stabilizer state close to $|\psi\rangle$ as long as $F_{\text{STAB}}(|\psi\rangle) > 1/2$. Thus, the approximate certification can give a non-trivial result as long as $M_2 \leq \ln(4/3)$.

Now, let us use the closest stabilizer state to certify the fidelity of random Hamiltonian evolution after time t . For evolved state $|\psi(t)\rangle$, for small t the closest stabilizer state is $|\psi(0)\rangle$. We have $M_2(t) \approx 4t^2$ and thus certification error scaling as $\Delta F \approx 4t$. Thus, one can certify the fidelity of $|\psi(t)\rangle$ with non-trivial error up to time $t \leq \frac{1}{4}$.

While M_2 is small for such t , note that this is not true for SREs with $\alpha < 1$. For example, $M_{1/2}(t) \approx \ln(2t^2) + N \ln(2) \sim N$ for any $t \gtrsim 1/\text{poly}(N)$.

Commonly, Pauli fidelity certification becomes inefficient when states have a lot of nonstabilizerness [30]. However, we argue that this statement applies strictly only for $\alpha > 1$. This is because there are two different aspects of nonstabilizerness: While $\alpha < 1$ relates to hardness of Clifford simulation, $\alpha > 1$ measures the distance to the closest stabilizer states.

For (approximate) Pauli fidelity estimation, where one checks the fidelity against the closest stabilizer state, the sampling complexity is related to the closest stabilizer state. As such, one can approximate the fidelity efficiently as long as the $\alpha = 2$ SRE M_2 is sufficiently small. This holds true even when $\alpha < 1$ SREs has become extensive.